Article

Relatives of rubella virus in diverse mammals

https://doi.org/10.1038/s41586-020-2812-9

Received: 12 October 2019

Accepted: 17 July 2020

Published online: 7 October 2020

Check for updates

Andrew J. Bennett[1,12], Adrian C. Paskey[2,3,4,12], Arnt Ebinger[5,12], Florian Pfaff[5], Grit Priemer[6], Dirk H˚ per[5], Angele Breithaupt[7], Elisa Heuser[8,9], Rainer G. Ulrich[8,9], Jens H. Kuhn[10], Kimberly A. Bishop-Lilly[2,4], Martin Beer[5]✉ & Tony L. Goldberg[1,11]✉

Since 1814, when rubella was first described, the origins of the disease and its causative agent, rubella virus (*Matonaviridae*: *Rubivirus*), have remained unclear[1]. Here we describe ruhugu virus and rustrela virus in Africa and Europe, respectively, which are, to our knowledge, the first known relatives of rubella virus. Ruhugu virus, which is the closest relative of rubella virus, was found in apparently healthy cyclops leaf-nosed bats (*Hipposideros cyclops*) in Uganda. Rustrela virus, which is an outgroup to the clade that comprises rubella and ruhugu viruses, was found in acutely encephalitic placental and marsupial animals at a zoo in Germany and in wild yellow-necked field mice (*Apodemus flavicollis*) at and near the zoo. Ruhugu and rustrela viruses share an identical genomic architecture with rubella virus[2,3]. The amino acid sequences of four putative B cell epitopes in the fusion (E1) protein of the rubella, ruhugu and rustrela viruses and two putative T cell epitopes in the capsid protein of the rubella and ruhugu viruses are moderately to highly conserved[4–6]. Modelling of E1 homotrimers in the post-fusion state predicts that ruhugu and rubella viruses have a similar capacity for fusion with the host-cell membrane[5]. Together, these findings show that some members of the family *Matonaviridae* can cross substantial barriers between host species and that rubella virus probably has a zoonotic origin. Our findings raise concerns about future zoonotic transmission of rubella-like viruses, but will facilitate comparative studies and animal models of rubella and congenital rubella syndrome.

Rubella, which was first described in 1814[7], is an acute, highly contagious human infectious disease that is typically characterized by a rash, low-grade fever, adenopathy and conjunctivitis[1]. Research from the 1940s to 1960s revealed that the contraction of rubella (also called "German measles") during the first trimester of pregnancy was directly associated with severe congenital birth defects, miscarriage and stillbirth[8,9]. Rubella virus (RuV), which is currently the only recognized member of the riboviriad family *Matonaviridae* (genus *Rubivirus*), is the aetiological agent of rubella[10,11] and causes fetal pathology after transplacental transmission[12]. Extensive rubella epidemics have occurred worldwide due to the high airborne transmissibility of RuV (R_0 = 3.5–7.8)[13]. Safe, efficacious, live-attenuated RuV vaccines, including the measles, mumps, rubella (MMR) vaccine, are now used worldwide and have successfully decreased the global incidence of rubella. However, around 100,000 cases of congenital rubella syndrome still occur annually[1], and RuV can persist in immunologically privileged anatomical sites (for example, the eye) for years[14]. Furthermore, RuV infection in adults is generally underreported, as 30–50% of cases of adults with RuV infections are subclinical[15]. High-priority areas for rubella vaccination include the western Pacific, eastern Mediterranean and African regions, where RuV circulates widely and primarily infects young children[16]. The elimination of RuV is considered to be rapidly achievable because of the effectiveness of available vaccines and the lack of known animal reservoirs[17,18].

Here we report the discovery of ruhugu virus (RuhV) and rustrela virus (RusV), which are relatives of RuV. RuhV was found in 10 out of 20 oral swabs from apparently healthy cyclops leaf-nosed bats (Hipposideridae: *Hipposideros cyclops* Temminck, 1853) in Kibale National Park, Uganda (Fig. 1). RusV was found in brain tissues of three acutely ill animals at a zoo in Germany, all of which succumbed to severe, acute neurological disease (Extended Data Table 2): a donkey (*Equus asinus* (Linnaeus, 1758)), a capybara (*Hydrochoeris hydrochaeris* Linnaeus, 1766) and a red-necked wallaby (*Macropus rufogriseus* Desmarest, 1817). RusV was subsequently detected in the brain tissues of 8 out of 16 yellow-necked field mice (Muridae: *Apodemus flavicollis* (Melchior, 1834)) on the zoo grounds and within 10 km of the zoo (Fig. 1 and Extended Data Table 1).

In the case of RuhV in Uganda, all bats were captured and sampled from five tree roosts (hollow cavities in trees) each of which contained between one and eight bats. Using molecular and metagenomic methods (Methods), RuhV RNA was detected in 5 out of 9 (55.6%) males and 5 out of 11 (45.5%) females in 4 out of 5 (80.0%) of the roosts (50% overall

[1]Department of Pathobiological Sciences, University of Wisconsin-Madison, Madison, WI, USA. [2]Department of Microbiology and Immunology, Uniformed Services University of the Health Sciences, Bethesda, MD, USA. [3]Leidos, Reston, VA, USA. [4]Genomics and Bioinformatics Department, Biological Defense Research Directorate, Naval Medical Research Center–Frederick, Fort Detrick, Frederick, MD, USA. [5]Institute of Diagnostic Virology, Friedrich-Loeffler-Institut, Greifswald-Insel Riems, Germany. [6]State Office for Agriculture, Food Safety and Fisheries, Rostock, Germany. [7]Department of Experimental Animal Facilities and Biorisk Management, Friedrich-Loeffler-Institut, Greifswald-Insel Riems, Germany. [8]Institute of Novel and Emerging Infectious Diseases, Friedrich-Loeffler-Institut, Greifswald-Insel Riems, Germany. [9]German Center for Infection Research (DZIF), Hamburg-L, beck-Borstel-Insel Riems, Greifswald-Insel Riems, Germany. [10]Integrated Research Facility at Fort Detrick, National Institute of Allergy and Infectious Diseases, National Institutes of Health, Fort Detrick, Frederick, MD, USA. [11]Global Health Institute, University of Wisconsin-Madison, Madison, WI, USA. [12]These authors contributed equally: Andrew J. Bennett, Adrian C. Paskey, Arnt Ebinger. ✉e-mail: martin.beer@fli.de; tony.goldberg@wisc.edu

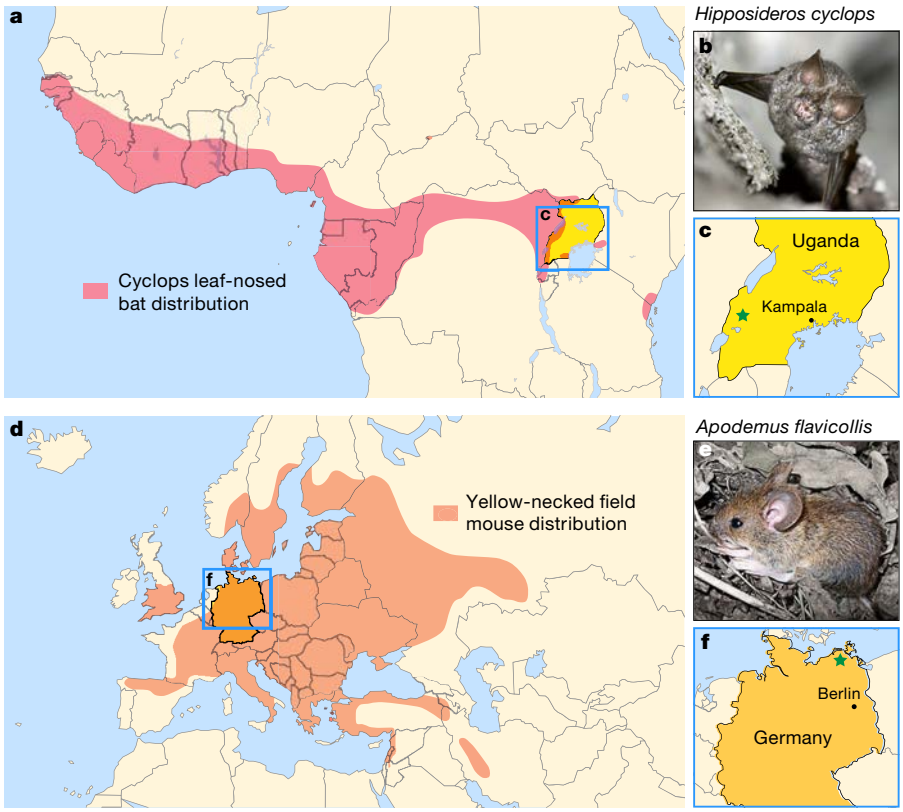

Fig. 1 | Geographical locations of viruses and their hosts. a, Summary map of the estimated distribution of the cyclops leaf-nosed bat in Africa (red) and Uganda (blue box). **b**, Cyclops leaf-nosed bat in Kibale National Park, Uganda. Photograph credit: C. Johnson. **c**, Location at which the bat sample was collected and the ruhugu virus was discovered (Kibale National Park, Uganda, green star). **d**, Summary map of the estimated distribution of the yellow-necked field mouse in Eurasia (orange) and Germany (blue box). **e**, Yellow-necked field mouse in northeastern Germany. Photograph credit: U. M. Rosenfeld. **f**, Location of the zoo animals and discovery of RusV in Germany (southern Baltic Sea region, green star).

prevalence; 95% confidence interval, 29.9–70.1%). This high prevalence and frequency of positive roosts suggest that apparently healthy cyclops leaf-nosed bats are reservoir hosts, rather than incidental hosts, of RuhV. Cyclops leaf-nosed bats are small insectivorous bats that are primarily found in lowland rainforests from Senegal to Tanzania but are also found in coastal, montane and swamp forests as well as disturbed and agricultural landscapes[19–21] (Fig. 1a), and are a host for *Plasmodium cyclopsi*, an apicomplexan bat malariaí parasite[22,23]. Whether RuhV can infect animals other than cyclops leaf-nosed bats remains unknown.

In the case of RusV in Germany, the donkey, capybara and red-necked wallaby were submitted for post-mortem evaluation and testing (Methods), which led to the identification of the virus (see below). Subsequent testing of rodents housed at the zoo and wild rodents on the zoo grounds and at two other locations within 10 km of the zoo revealed that 8 out of 16 (50%; 95% confidence interval 6.7–39.1%) yellow-necked field mice were positive for RusV RNA in brain tissue. Notably, the mice had no histological evidence of encephalitis (7 out of 8 mice investigated) and had only low concentrations of RusV RNA in peripheral organs (Extended Data Table 3). RusV RNA was not detected in any other small mammals collected simultaneously ($n = 38$; Extended Data Table 1). Yellow-necked field mice are omnivorous rodents that are native to parts of Europe and Asia, occupying habitats that range from mature forests to agricultural and peridomestic environments[24] (Fig. 1d). They are a host of tick-borne encephalitis virus (*Flaviviridae*: *Flavivirus*)[25], Dobrava virus (*Hantaviridae*: *Orthohantavirus*)[26–28], Akhmeta virus (*Poxviridae*: *Orthopoxvirus*)[29] and hepatitis E virus (*Hepeviridae*: *Orthohepevirus*)[30]. Routes of transmission of RuhV and RusV between reservoir hosts and to spill-over hosts (in the case of RusV) remain unknown, but the presence of the virus in oral swabs and faeces (Extended Data Table 3) suggests that contact with oral secretions and excreta could have a role.

Using molecular methods and in situ hybridization (Methods), we confirmed the presence of RusV in the brain tissues of all German zoo animals and in the liver of the donkey (Extended Data Table 2 and Extended Data Fig. 1). RusV RNA was detected within neuronal cell bodies and their processes in brain tissue sections of the donkey (Extended Data Fig. 1a), red-necked wallaby (Extended Data Fig. 1b) and capybara (Extended Data Fig. 1c) using in situ RNA hybridization. Histopathology revealed a nonsuppurative meningoencephalitis in all three animals, which was characterized by perivascular cuffing (Fig. 2a–c), meningeal infiltrates (Fig. 2d) and glial nodules (Fig. 2e). Neuronal necrosis and degeneration with satellitosis were detected in the brain stem of the donkey (Fig. 2f). Immune cells in the brain tissue consisted mainly of CD3-positive T lymphocytes, IBA-1-positive microglial cells and macrophages, and CD79a-immunoreactive B lymphocytes (Fig. 2g–l). In general, apoptosis was not a marked feature; only a few active-caspase-3-labelled cells were found to be distributed perivascularly and scattered within the grey and white matter (Fig. 2m, n). Multifocal perivascular red blood cells in the brain samples of the donkey and red-necked wallaby were positive for iron, as shown by Prussian Blue staining, which is indicative of intra-vital haemorrhages (Fig. 2o). The detection of viral RNA in samples from yellow-necked field mice collected between 2009 and 2020 and the absence of inflammation in the mice (Extended Data Fig. 1d, e) suggest that this broadly distributed rodent is the reservoir host of RusV.

The genome organizations of RuV, RuhV and RusV are identical, consisting of two large open-reading frames (ORFs), two untranslated regions at the 5′ and 3′ termini, and an intergenic region between

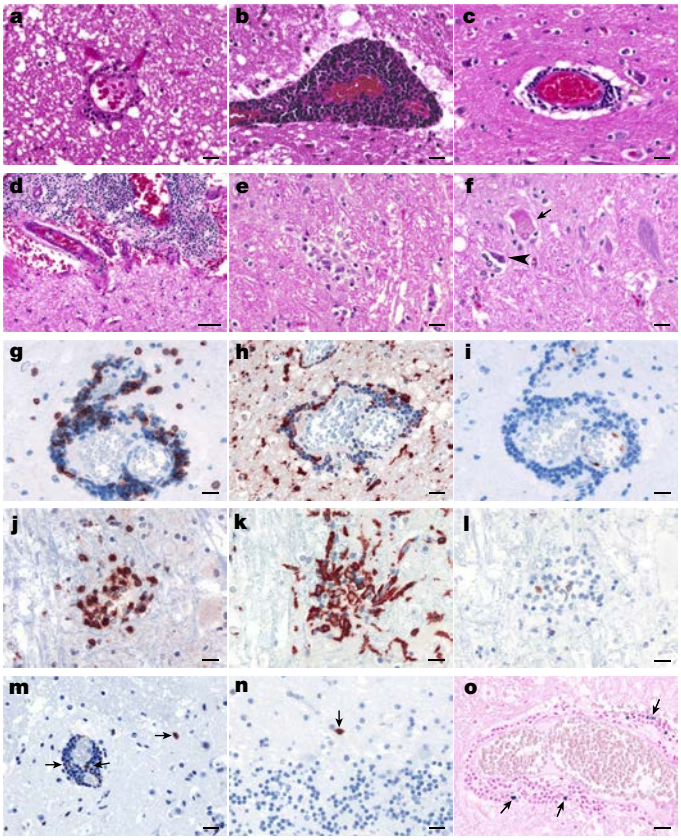

Fig. 2 | Histopathology and immune reaction of RusV in the brain of a capybara, red-necked wallaby and donkey. a–c, Nonsuppurative meningoencephalitis with mononuclear perivascular cuffing in the brain of a capybara (**a**), red-necked wallaby (**b**) and donkey (**c**). **d**, Mononuclear meningeal infiltrates in the brain of a donkey. **e**, Glial nodules in the brain of a donkey. **f**, Neuronal necrosis (arrow) and degeneration with satellitosis (arrowhead) in the brain of a donkey. Haematoxylin and eosin was used. Scale bars, 20 µm (**a–c**, **e**, **f**) and 50 µm (**d**). **g–l**, Immunohistochemistry images of the immune reaction, in the perivascular tissue of the brain of a red-necked wallaby (**g–i**) and in glial nodules of the brain of a donkey (**j–l**). Numerous CD3-labelled T lymphocytes (**g**, **j**), IBA-1-positive microglial cells and macrophages (**h**, **k**) and CD79a-immunoreactive B lymphocytes (**i**, **l**) are shown. Immunohistochemistry was performed using AEC chromogen counterstained with Mayer's haematoxylin. Scale bars, 20 µm. **m**, **n**, Apoptosis, indicated by few active-caspase-3-labelled cells (arrows) found in the perivascular tissue and scattered throughout the neuropil in the brain of a red-necked wallaby (**m**) and capybara (**n**). Immunohistochemistry was performed using AEC chromogen counterstained with Mayer's haematoxylin. Scale bars, 20 µm. **o**, The Prussian Blue reaction highlights multiple iron deposits (arrows) within mononuclear cells that were found in perivascular tissue, mixed with accumulations of red blood cells, which is indicative of an intra-vital haemorrhage. Scale bar, 20 µm. Immunohistochemistry was performed on at least four slides per animal, yielding comparable results in all cases. In each run, positive control slides and a negative control for the primary antibodies were included. Evaluation and interpretation were performed by a board-certified pathologist (DiplECVP) with more than 13 years of experience.

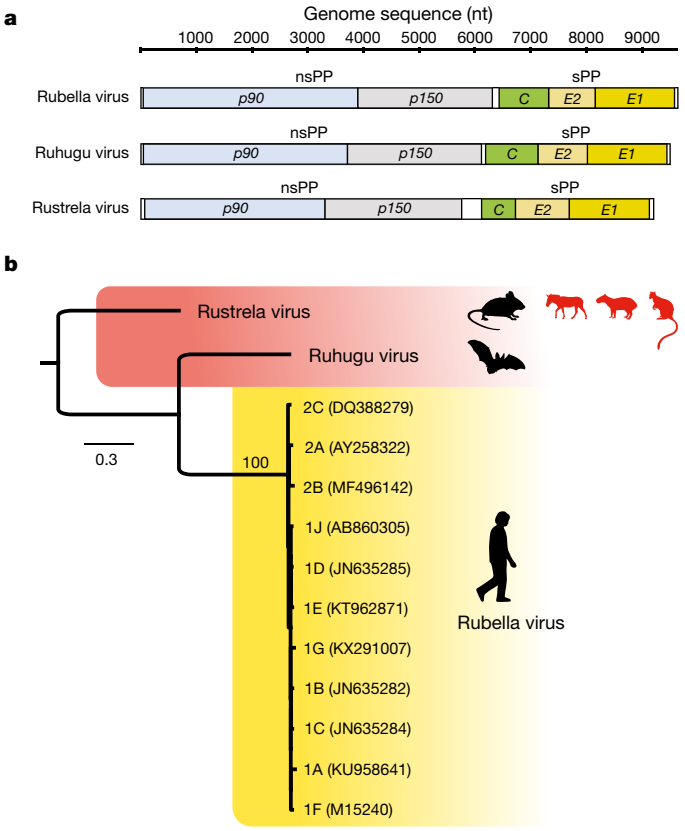

Fig. 3 | Evolutionary relationships among viruses. a, Comparative genome architecture of RuV, RuhV and RusV, showing five ORFs (coloured), two untranslated regions at the 5′ and 3′ termini (white) and an intergenic region (white) between the ORFs that encode the non-structural (nsPP) and structural (sPP) polyproteins. **b**, Maximum likelihood phylogenetic tree of RusV, RuhV and RuV genotypes 1A–1J and 2A–2C. Black silhouettes represent the natural hosts of each virus, and red silhouettes represent spill-over hosts in the case of RusV. Numbers beside nodes indicate bootstrap values (as a percentage; only values for major branches are shown); the scale bar indicates the number of amino acid substitutions per site.

the two ORFs (Fig. 3a). Across the non-structural and structural polyprotein-coding regions, RuhV is more similar to RuV than is RusV (Extended Data Table 4). Genetic similarity varies within the coding regions and is generally highest in a hyperconserved region within the Y domain of p150[2,31,32] (Extended Data Fig. 2). RusV contains a markedly long intergenic region (366 nucleotides, compared with 46 nucleotides and 75 nucleotides in RuV and RuhV, respectively) and a correspondingly short C protein (205 amino acids, compared with 300 amino acids and 317 amino acids in RuV and RuhV, respectively; Extended Data Table 4). In addition, RuV and RuhV share a Gly-Gly-Gly amino acid sequence at the p150/p90 cleavage site, whereas RusV has a Gly-Gly-Ala amino acid sequence at this same site, which may impair cleavage in the case of RusV[3].

RuhV (named for Ruteete subcounty, Uganda, and the Tooro word for insectivorous bat, *obuhuguhugu*) is an outgroup to all known RuV genotypes (Fig. 3b). RusV (named for its rubella virus-like genome and the Strelasund of the Baltic Sea in Germany) is a close outgroup to the clade comprising RuV and RuhV (Fig. 3b). This topology is consistent with the higher similarity of RuhV to RuV in each of the five mature polypeptides of the protein-coding viral genome (Extended Data Table 4 and Extended Data Fig. 2). Nucleotide sequences of RusV were 97.4–100% similar within the coding regions of the p90 and E1 genes sequenced in the samples from the donkey, capybara, red-necked wallaby and yellow-necked field mice in Germany (Extended Data Fig. 3).

The RuV E1 protein, a receptor-binding, class-II fusion protein[5], contains an immune-reactive region (amino acid residue positions 202–283) with immunodominant T cell epitopes[6] and four linear, neutralizing B cell epitopes (NT1–NT4)[4] (Fig. 4a). The modelled tertiary and quaternary structures of trimeric E1 proteins of RuhV and RusV are homologous to the E1 protein of RuV[33], and homology-based modelling of the quaternary structure of the E1 protein of RuhV predicts with high confidence that the E1 proteins of RuhV and RusV form homotrimers in the post-fusion state[5] (Fig. 4b, c). One neutralizing epitope maps

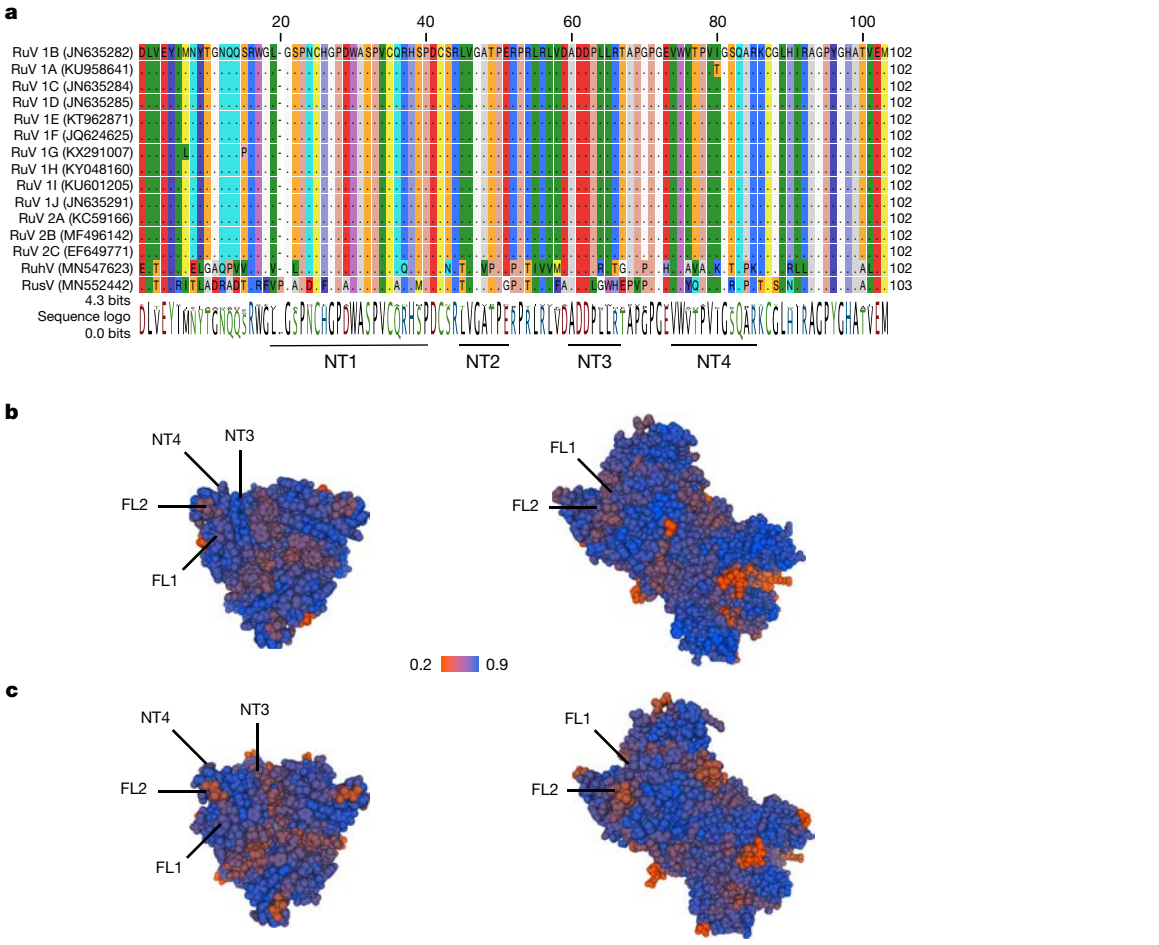

Fig. 4 | Comparisons of the E1 envelope glycoproteins of RuV, RuhV and RusV. a, Amino acid alignment and sequence logo of an immunoreactive region of E1 for RuhV, RusV and 13 RuV genotypes (GenBank accession numbers are included in parentheses). Lines indicate the locations of putative linear neutralizing B cell epitopes NT1ñNT4. **b**, Homology≠based model of the structure of the E1 homotrimer of RuhV in the post≠fusion state, showing the receptor≠binding site view (left) and profile view (right). Global model quality estimates (QMEAN) indicate a good model fit relative to the crystal structure of the E1 protein of RuV in the post≠fusion form (Protein Data Bank biological assembly 4ADG_1). **c**, Homology≠based model of the structure of the E1 homotrimer of RusV in the post≠fusion state, as described above for RuhV. Key differences are seen in the modelled neutralizing epitopes NT3 and NT4 and in fusion loops 1 and 2 (FL1 and FL2). Residues of FL1 and FL2 of RuhV residues are highly similar to those of RuV, whereas FL2 residues of RusV differ from those of FL2 of RuV to a greater extent. The colour scale indicates the normalized QMEAN local score.

to amino acid positions 223ñ239 of the E1 protein at disulfide bond 8 (NT1)[34]. The mechanism of neutralization appears to involve block≠ing the trimerization of E1, which is necessary for virion fusion with the plasma membrane of the host cell[5]. Notably, only one amino acid residue (R237Q, near the C terminus) differs between the RuV and RuhV NT1 epitope (Fig. 4a), despite higher divergence at the amino acid level across E1 (Extended Data Fig. 3). By contrast, RusV differs from RuV at five amino acid residues within the same region (Fig. 4a). T cell epitopes are not well conserved in the capsid protein (Extended Data Table 5); however; the exposed putative linear epitopes of NT3 and NT4 in the E1 protein of RuhV and RusV are moderately conserved in comparison to RuV (Fig. 4 and Extended Data Table 5), suggesting that they should also be evaluated for cross≠neutralization by anti≠RuV antibodies.

The fusion loops (FL1, residues 87ñ92; FL2, residues 130ñ136) in the E1 protein of RuhV are predicted to support the unusual metal ion com≠plex that is necessary for E1≠mediated RuV membrane fusion due to the presence in RuhV of amino acids N87 and D135 (homologous to RuV N88 and N136, respectively[5]; Fig. 4b). By contrast, FL2 of RusV is predicted to be less similar to RuV due to two amino acid residue replacements, P134A and T135A, the latter of which comprises a change from a polar to a non≠polar residue (Fig. 4c). Across the RuV, RuhV and RusV genomes, regions of marked conservation and stabilizing selection are evident immediately upstream of the putative methyltransferase domain of p150, in the RdRp domain of p90, and proximal to the aforementioned NT1 epitope of E1 (Extended Data Fig. 2).

The similarity or near identity of certain RuV, RuhV and RusV B cell epitopes (Extended Data Table 5) suggests that existing serological assays for anti≠rubella antibodies might detect RuhV, RusV and other as≠yet≠undescribed RuV≠like viruses. Future studies that evaluate the performance of existing serological tests for RuV infection in animals would be useful, as would the development of new assays that can detect and differentiate among rubella≠like viral infections in animals and humans. The implication that RuhV or RusV are zoonotic agents is currently speculative; however, bats and rodents possess biological attributes that predispose them to hosting many zoonotic viruses[35ñ37], so this scenario should not be dismissed. The ability of RusV to infect both placental and marsupial mammals and to cause disease symptoms that resemble the severe encephalitic forms of rubella in humans[38,39] reinforces such a precautionary stance.

The Global Measles and Rubella Strategic Plan of the World Health Organization (WHO) aims to control or eliminate rubella and congenital rubella syndrome in 5 out of 6 WHO regions by the end of 2020[40]. Our discovery of relatives of RuV that infect asymptomatic bats and rodents suggests that rubella may have arisen as a zoonosis. Furthermore, the

ability of RusV to infect mammals across wide taxonomic distances and to cause severe encephalitis in spill≠over hosts raises concern about the potential for zoonotic transmission of RuhV, RusV or other RuV≠like viruses. Despite these concerns, our findings will facilitate compara≠tive studies of RuV that were previously not possible, including the potential development of animal models of rubella and congenital rubella syndrome.

Online content

Any methods, additional references, Nature Research reporting sum≠maries, source data, extended data, supplementary information, acknowledgements, peer review information; details of author con≠tributions and competing interests; and statements of data and code availability are available at https://doi.org/10.1038/s41586≠020≠2812≠9.

1. Lambert, N., Strebel, P., Orenstein, W., Icenogle, J. & Poland, G. A. Rubella. *Lancet* **385**, 2297ñ2307 (2015).
2. Zhou, Y., Ushijima, H. & Frey, T. K. Genomic analysis of diverse rubella virus genotypes. *J. Gen. Virol.* **88**, 932ñ941 (2007).
3. Chen, J.≠P., Strauss, J. H., Strauss, E. G. & Frey, T. K. Characterization of the rubella virus nonstructural protease domain and its cleavage site. *J. Virol.* **70**, 4707ñ4713 (1996).
4. Perelygina, L. et al. Infectious vaccine≠derived rubella viruses emerge, persist, and evolve in cutaneous granulomas of children with primary immunodeficiencies. *PLoS Pathog.* **15**, e1008080 (2019).
5. DuBois, R. M. et al. Functional and evolutionary insight from the crystal structure of rubella virus protein E1. *Nature* **493**, 552ñ556 (2013).
6. McCarthy, M., Lovett, A., Kerman, R. H., Overstreet, A. & Wolinsky, J. S. Immunodominant T≠cell epitopes of rubella virus structural proteins defined by synthetic peptides. *J. Virol.* **67**, 673ñ681 (1993).
7. Maton, W. G. Some account of a rash liable to be mistaken for scarlatina. *Med. Trans. R. Coll. Physicians* **5**, 149ñ165 (1815).
8. Cooper, L. Z. The history and medical consequences of rubella. *Rev. Infect. Dis.* **7**, S2ñS10 (1985).
9. Gregg, N. M. Congenital cataract following German measles in the mother. *Aust. N. Z. J. Ophthalmol.* **3**, 35ñ46 (1941).
10. Parkman, P. D., Buescher, E. L. & Artenstein, M. S. Recovery of rubella virus from army recruits. *Proc. Soc. Exp. Biol. Med.* **111**, 225ñ230 (1962).
11. Weller, T. H. & Neva, F. A. Propagation in tissue culture of cytopathic agents from patients with rubella≠like illness. *Proc. Soc. Exp. Biol. Med.* **111**, 215ñ225 (1962).
12. Swan, C., Tostevin, A. L. & Black, G. H. Final observations on congenital defects in infants following infectious diseases during pregnancy, with special reference to rubella. *Med. J. Aust.* **2**, 889ñ908 (1946).
13. Edmunds, W. J., Gay, N. J., Kretzschmar, M., Pebody, R. G. & Wachmann, H. The pre≠vaccination epidemiology of measles, mumps and rubella in Europe: implications for modelling studies. *Epidemiol. Infect.* **125**, 635ñ650 (2000).
14. Gonzales, J. A. et al. Association of ocular inflammation and rubella virus persistence. *JAMA Ophthalmol.* **137**, 435ñ438 (2019).
15. Grant, G. B., Reef, S. E., Patel, M., Knapp, J. K. & Dabbagh, A. Progress in rubella and congenital rubella syndrome control and elimination ó worldwide, 2000ñ2016. *MMWR Morb. Mortal. Wkly. Rep.* **66**, 1256ñ1260 (2017).
16. Namuwulya, P. et al. Phylogenetic analysis of rubella viruses identified in Uganda, 2003ñ2012. *J. Med. Virol.* **86**, 2107ñ2113 (2014).
17. Kretsinger, K., Strebel, P., Kezaala, R. & Goodson, J. L. Transitioning lessons learned and assets of the global polio eradication initiative to global and regional measles and rubella elimination. *J. Infect. Dis.* **216**, S308ñS315 (2017).
18. Wolfe, N. D., Dunavan, C. P. & Diamond, J. Origins of major human infectious diseases. *Nature* **447**, 279ñ283 (2007).
19. Fahr, J. in *Mammals of Africa. Vol. IV: Hedgehogs, Shrews and Bats* (eds Happold, M. & Happold, D. C. D.) 380ñ383 (Bloomsbury, 2013).
20. Jetz, W., McPherson, J. M. & Guralnick, R. P. Integrating biodiversity distribution knowledge: toward a global map of life. *Trends Ecol. Evol.* **27**, 151ñ159 (2012).
21. OíShea, T. J., Bogan, M. A. & Ellison, L. E. *Monitoring Trends in Bat Populations of the United States and Territories: Status of the Science and Recommendations for the Future*. Information and Technology Report USGS/BRD/ITRñ2003ñ0003 (US Department of the Interior, US Geological Survey Washington, 2003).
22. Landau, I. & Chabaud, A.≠G. Description de *Plasmodium cyclopsi* n. sp. parasite du MicrochirotËre *Hipposideros cyclops* ‡ Makokou (Gabon). *Ann. Parasitol. Hum. Comp.* **53**, 247ñ253 (1978).
23. Schaer, J. et al. High diversity of West African bat malaria parasites and a tight link with rodent *Plasmodium* taxa. *Proc. Natl Acad. Sci. USA* **110**, 17415ñ17419 (2013).
24. Michaux, J. R., Libois, R. & Filippucci, M.≠G. So close and so different: comparative phylogeography of two small mammal species, the yellow≠necked fieldmouse (*Apodemus flavicollis*) and the woodmouse (*Apodemus sylvaticus*) in the Western Palearctic region. *Heredity* **94**, 52ñ63 (2005).
25. Labuda, M. et al. Tick≠borne encephalitis virus transmission between ticks cofeeding on specific immune natural rodent hosts. *Virology* **235**, 138ñ143 (1997).
26. Klempa, B. et al. Complex evolution and epidemiology of DobravañBelgrade hantavirus: definition of genotypes and their characteristics. *Arch. Virol.* **158**, 521ñ529 (2013).
27. Sibold, C. et al. Dobrava hantavirus causes hemorrhagic fever with renal syndrome in central Europe and is carried by two different *Apodemus* mice species. *J. Med. Virol.* **63**, 158ñ167 (2001).
28. Oktem, I. M. et al. DobravañBelgrade virus in *Apodemus flavicollis* and *A. uralensis* mice, Turkey. *Emerg. Infect. Dis.* **20**, 121ñ125 (2014).
29. Doty, J. B. et al. Isolation and characterization of Akhmeta virus from wild≠caught rodents (*Apodemus* spp.) in Georgia. *J. Virol.* **93**, e00966≠19 (2019).
30. Prpić, J. et al. First evidence of hepatitis E virus infection in a small mammal (yellow≠necked mouse) from Croatia. *PLoS ONE* **14**, e0225583 (2019).
31. Hofmann, J., Renz, M., Meyer, S., von Haeseler, A. & Liebert, U. G. Phylogenetic analysis of rubella virus including new genotype I isolates. *Virus Res.* **96**, 123ñ128 (2003).
32. Abernathy, E. et al. Analysis of whole genome sequences of 16 strains of rubella virus from the United States, 1961ñ2009. *Virol. J.* **10**, 32 (2013).
33. Kelley, L. A., Mezulis, S., Yates, C. M., Wass, M. N. & Sternberg, M. J. E. The Phyre2 web portal for protein modeling, prediction and analysis. *Nat. Protocols* **10**, 845ñ858 (2015).
34. Wolinsky, J. S. et al. An antibody≠and synthetic peptide≠defined rubella virus E1 glycoprotein neutralization domain. *J. Virol.* **67**, 961ñ968 (1993).
35. Guy, C., Thiagavel, J., Mideo, N. & Ratcliffe, J. M. Phylogeny matters: revisiting ëa comparison of bats and rodents as reservoirs of zoonotic virusesí. *R. Soc. Open Sci.* **6**, 181182 (2019).
36. Luis, A. D. et al. A comparison of bats and rodents as reservoirs of zoonotic viruses: are bats special? *Proc. R. Soc. Lond. B* **280**, 20122753 (2013).
37. Olival, K. J. et al. Host and viral traits predict zoonotic spillover from mammals. *Nature* **546**, 646ñ650 (2017).
38. Frey, T. K. Neurological aspects of rubella virus infection. *Intervirology* **40**, 167ñ175 (1997).
39. Bharadwaj, S. D. et al. Acute encephalitis with atypical presentation of rubella in family cluster, India. *Emerg. Infect. Dis.* **24**, 1923ñ1925 (2018).
40. Grant, G. B. et al. Accelerating measles and rubella elimination through research and innovation ó findings from the Measles & Rubella Initiative research prioritization process, 2016. *Vaccine* **37**, 5754ñ5761 (2019).

Publisherís note Springer Nature remains neutral with regard to jurisdictional claims in published maps and institutional affiliations.

© The Author(s), under exclusive licence to Springer Nature Limited 2020

Methods

Data reporting

No statistical methods were used to predetermine sample size. The experiments were not randomized and the investigators were not blinded to allocation during experiments and outcome assessment.

Animal sampling and pathology

In Uganda, cyclops leaf-nosed bats were captured and released in Kibale National Park from June to July 2017. Kibale is a 795-km^2 mid-altitude semideciduous forest park (0°13′–0°41″ N, 30°19′–30°31″ E)[41] within the Albertine Rift, which is a region of exceptional biodiversity[42] (Fig. 1c). Bats were caught in mist nets (Avinet) set in their flight path as they exited tree roosts at dusk and were kept in cloth bags until processing. Oral swabs were collected from each bat using sterile rayon-polyester-tipped swabs and preserved in 500 µl of TRI Reagent (Zymo Research). Swabs were frozen at −20 °C within 3 h of sample collection and transported on ice for storage at −80 °C before analysis. Animal collection and handling protocols were approved by the Uganda Wildlife Authority, the Uganda National Council for Science and Technology, and the University of Wisconsin-Madison Animal Care and Use Committee. Samples were shipped in accordance with international law and imported under PHS permit number 2017-07-103 issued by the US Centers for Disease Control and Prevention.

In Germany, a donkey, a capybara and a red-necked wallaby were submitted for necropsy from July 2018 to October 2019 after presenting with acute and severe neurological signs, including ataxia, convulsions, lethargy and unresponsiveness. All animals were housed at the same small zoo close to the Baltic Sea coast in northeast Germany (Fig. 1f). Standard diagnostic tests were negative for rabies virus, bornaviruses, West Nile virus, herpesviruses, *Listeria*, *Salmonella* and *Toxoplasma*. Formalin-fixed, paraffin-embedded (FFPE) brain tissues (cerebral cortex, cerebellum, brain stem and medulla oblongata) were cut at 3-µm thickness and stained with haematoxylin and eosin for examination using light microscopy. Conventional Prussian Blue staining was performed to demonstrate the presence of ferric iron, which indicates haemosiderin. Immunohistochemistry for immune cell markers was performed according to standardized procedures (Extended Data Table 6), and bright red intracytoplasmic chromogen labelling was produced with 3-amino-9-ethylcarbazole substrate (AEC, DAKO). Sections were counterstained with Mayer's haematoxylin.

In situ hybridization for the detection of RusV RNA in brain tissue sections was performed with the RNAScope 2-5 HD Reagent Kit-Red (Advanced Cell Diagnostics) according to the manufacturer's instructions. For hybridization, RNAScope probes were custom-designed against the RusV non-structural protein gene. The specificity of the probes was verified using a positive control probe against peptidylprolyl isomerase B (cyclophilin B) and a negative control probe against dihydrodipicolinate reductase (DapB). Histopathology and RNAScope interpretation were performed by a board-certified pathologist (DiplECVP).

Rodent management on the zoo grounds and hygiene measures for zoo staff were intensified after detection of a RusV infection in the deceased zoo animals. From September 2019 to February 2020, a total of 29 muroid rodents were collected from the grounds of the zoo (Extended Data Table 1). In addition, two brown rats (*Rattus norvegicus*) and three house mice (*Mus musculus*) housed at the zoo were sampled. Additional wild rodent samples were collected or retrieved from freezer archives from two trapping sites within 10 km of the zoo, where long-term research on rodent-borne pathogens is being conducted[43]. All wild-caught rodent species identifications were confirmed by cytochrome *b* DNA barcoding[44]. The zoo does not house bats and bats of the genus *Hipposideros* do not inhabit Germany. However, bats of the related and comparably speciose genus *Rhinolophus* do inhabit Germany and probably occur on or near the zoo grounds[45].

All work with live animals and animal tissues was performed in compliance with all relevant ethical regulations.

Metagenomic, molecular and bioinformatic analyses

RNA was purified from bat oral swabs using the Direct-zol RNA MicroPrep kit (Zymo Research). RNA TruSeq libraries were then prepared, evaluated for quality, multiplexed and sequenced with NextSeq 500 v.2 chemistry using 2 × 150-bp cartridges (Illumina). RuhV was first identified using the VirusSeeker virus discovery pipeline[46], after which deeper sequencing of two bat swab libraries was performed on a MiSeq (Illumina) sequencer using v.3 chemistry and 2 × 300-bp read lengths. The cyclops leaf-nosed bat genome was removed in silico by mapping reads to assembly PVLB01000001 using bbmap v37.78[47] and discarding mapped reads. Non-viral reads were removed using FastQC v.0.11.5, bbmap v.37.78 and bbduk v.37.78[47,48], and de novo assembly was then performed using metaSPAdes[49]. Reads were then mapped back to contigs for validation, related viruses were identified by DIAMOND using the BlastX algorithm[49–51], and results were visualized using MEGAN v.6[52]. Detailed analyses of contigs and reads were performed with CLC Genomics Workbench v.12 (QIAGEN).

Initially, red-necked wallaby and donkey tissues were processed using published methods for metagenomic pathogen detection[53]. In brief, tissues were first disrupted using the Covaris cryoPREP system (Covaris) and subsequently lysed in buffer AL (QIAGEN), followed by addition of TRIzol reagent (Life Technologies). After centrifugation, the aqueous phase was then transferred to RNeasy Mini kit columns (QIAGEN) and processed according to the manufacturer's instructions, including on-column DNase treatment. Total RNAs from the cerebra of the donkey and the red-necked wallaby were used for library preparation[53] and sequencing on an Ion S5 XL System with a 530 chip (Thermo Fisher Scientific). The RIEMS software pipeline[54] was used for initial taxonomic assignment of reads.

After RusV RNA was confirmed in the donkey using the methods described above, deeper sequencing was performed on an Ion S5 XL System and a MiSeq (Illumina). The donkey genome was removed in silico by mapping reads to assembly ASM130575v1 using BWA[55], and unmapped reads were filtered and retained. Read data quality trimming, adaptor removal and quality control were performed using the 454 software suite v.3.0 (Roche) and FastQC v.0.11.5[48]. De novo assembly was performed using SPAdes v.3.12.0[56]. RusV-specific contigs were then identified by DIAMOND using the BlastX algorithm[51] followed by iterative mapping and assembly using the 454 software suite, SPAdes v.3.12.0 and Bowtie 2 v.2.3.5.1[57] for contig extension and verification. Results were visualized using Geneious (v.11.1.5, Biomatters). ORFs were identified by ORF Finder (implemented in Geneious). Conserved elements were identified by translated amino acid sequence alignment to RuV genomes using MUSCLE and subsequent annotation of p150, p90 and E1. The 5′ end of E2 was identified by the similar hydrophobicity and sequence pattern of the E2 signal peptide of RuV[58] located at the C terminus of the capsid protein using ProtScale[59] (window size 3; relative weight for window edges 100%; weight variation model linear). The 5′ terminus of the RusV genome was sequenced by rapid amplification of cDNA ends (RACE) using RNA from the donkey brain samples along with a 5′ RACE system v2 (Invitrogen) and specific primers.

FFPE brain tissues and peripheral organ samples from the donkey, capybara, red-necked wallaby, and wild-caught and zoo-housed rodents were assayed for RusV using an original one-step real-time quantitative reverse-transcription PCR (RT–qPCR). Total RNA from FFPE tissues was extracted using a combination of the Covaris truXTRAC FFPE total NA kit and the Agencourt RNAdvance Tissue Kit (Beckman Coulter). Nucleic acid extraction from unfixed rodent tissues was performed using the KingFisher 96 Flex Workstation (Thermo Fisher Scientific) and the NucleoMagVET kit (Macherey-Nagel) according to the manufacturer's instructions. RT–qPCR was then performed using the SensiFAST Probe No-ROX One-Step kit (Bioline) with forward primer (1072–1091, 5′-CGAGCGTGTCTACAAGTTCA-3′), reverse primer (1219–1237, 5′-GACCATGATGTTGGCGAGG-3′) and 5′ probe (1161–1178,

5′-FAM-CCGAGGAGGACGCCCTGTGC-BHQ-1-3′) on a Bio-Rad CFX96 qPCR instrument (Bio-Rad). Primer and probe specificity were verified by BLASTn[51] in silico analyses and Sanger sequencing of amplicons (Eurofins Genomics Germany), with the β-actin (*Actb*) gene used as an internal inhibition control. DNase digestion and RNA purification of nucleic acids of RusV-positive yellow-necked field mouse brain tissues (KS20/923, KS20/928, KS20/1296, KS20/1340, KS20/1341, KS20/1342, KS20/1343 and Mu09/1341) were performed using the Agencourt RNA-dvance Tissue kit or RNeasy Mini kit RNA clean-up protocol (QIAGEN). Total RNAs from the capybara and mice were then used for cDNA synthesis and library preparation (200-bp fragments) and sequenced on a Ion S5 XL System with an Ion 540 chip[60]. RusV consensus sequences were determined by iterative mapping and assembly with the 454 software suite v.3.0 with reference to the RusV sequence derived from the donkey (GenBank MN552442).

Phylogenetic analyses and predictions of protein functional domains

To characterize relationships among RuhV, RusV and known RuV genotypes (Fig. 3b), coding sequences of non-structural and structural polyproteins were first concatenated and aligned using MAFFT v.7.388. A phylogenetic tree of aligned amino acid sequences was then inferred using IQ-TREE software v.1.6.12[61], with automated model selection (JTTDCMut+F+R3) and 500,000 ultrafast bootstrap replicates[62]. Phylogenetic analyses of the envelope glycoprotein E1 and the helicase and RNA-directed RNA polymerase p90 (Extended Data Fig. 3a, b) were conducted as described above.

Prediction and annotation of the functional domain of proteins from RuhV and RusV were performed using the InterPro webserver[63], and the confidence of E1 structural homology was estimated using Phyre2[33]. Homology modelling of the quaternary structure of the post-fusion E1 homotrimer (Fig. 2c, d) was performed using the SWISS-MODEL workspace[64] with model view by NGL[65] and the residue colour corresponds to the local QMEAN score[66], with 53 C-terminal residues of E1 (representing the stem and transmembrane segment of the E1 linear peptide) removed before homotrimer modelling[5]. Patterns of selection across the RuV, RuhV and RusV genomes were examined using SNAP 2.1.1[67,68].

Reporting summary

Further information on research design is available in the Nature Research Reporting Summary linked to this paper.

Data availability

Sequence data that support the findings of this study have been deposited in GenBank (accession numbers MN547623, MN552442 and MT274724–MT274737).

41. Struhsaker, T. T. *Ecology of an African Rain Forest: Logging in Kibale and the Conflict between Conservation and Exploitation* (Univ. Press Florida, 1997).
42. Plumptre, A. J. et al. The biodiversity of the Albertine Rift. *Biol. Conserv*. **134**, 178–194 (2007).
43. Ulrich, R. G. et al. Network ‘rodent-borne pathogens’ in Germany: longitudinal studies on the geographical distribution and prevalence of hantavirus infections. *Parasitol. Res*. **103**, S121–S129 (2008).
44. Schlegel, M. et al. Molecular identification of small mammal species using novel cytochrome *b* gene-derived degenerated primers. *Biochem. Genet*. **50**, 440–447 (2012).
45. Foley, N. M. et al. How and why overcome the impediments to resolution: lessons from rhinolophid and hipposiderid bats. *Mol. Biol. Evol*. **32**, 313–333 (2015).
46. Zhao, G. et al. VirusSeeker, a computational pipeline for virus discovery and virome composition analysis. *Virology* **503**, 21–30 (2017).
47. Bushnell, B. BBMap: a fast, accurate, splice-aware aligner. Version 37.78 https://sourceforge.net/projects/bbmap/ (2014).
48. Andrews, S. FastQC. A quality control tool for high throughput sequence data. Version 0.11.5 https://www.bioinformatics.babraham.ac.uk/projects/fastqc/ (2010).
49. Nurk, S., Meleshko, D., Korobeynikov, A. & Pevzner, P. A. metaSPAdes: a new versatile metagenomic assembler. *Genome Res*. **27**, 824–834 (2017).
50. Buchfink, B., Xie, C. & Huson, D. H. Fast and sensitive protein alignment using DIAMOND. *Nat. Methods* **12**, 59–60 (2015).
51. Altschul, S. F., Gish, W., Miller, W., Myers, E. W. & Lipman, D. J. Basic local alignment search tool. *J. Mol. Biol*. **215**, 403–410 (1990).
52. Huson, D. H. et al. MEGAN community edition – interactive exploration and analysis of large-scale microbiome sequencing data. *PLOS Comput. Biol*. **12**, e1004957 (2016).
53. Wylezich, C., Papa, A., Beer, M. & Höper, D. A versatile sample processing workflow for metagenomic pathogen detection. *Sci. Rep*. **8**, 13108 (2018).
54. Scheuch, M., Höper, D. & Beer, M. RIEMS: a software pipeline for sensitive and comprehensive taxonomic classification of reads from metagenomics datasets. *BMC Bioinformatics* **16**, 69 (2015).
55. Li, H. & Durbin, R. Fast and accurate short read alignment with Burrows–Wheeler transform. *Bioinformatics* **25**, 1754–1760 (2009).
56. Bankevich, A. et al. SPAdes: a new genome assembly algorithm and its applications to single-cell sequencing. *J. Comput. Biol*. **19**, 455–477 (2012).
57. Langmead, B. & Salzberg, S. L. Fast gapped-read alignment with Bowtie 2. *Nat. Methods* **9**, 357–359 (2012).
58. Hobman, T. C. & Gillam, S. In vitro and in vivo expression of rubella virus glycoprotein E2: the signal peptide is contained in the C-terminal region of capsid protein. *Virology* **173**, 241–250 (1989).
59. Gasteiger, E. et al. in *The Proteomics Protocols Handbook* (ed Walker, J. M.) 571–607 (Humana Press, 2005).
60. Forth, L. F. & Höper, D. Highly efficient library preparation for ion torrent sequencing using Y-adapters. *Biotechniques* **67**, 229–237 (2019).
61. Nguyen, L.-T., Schmidt, H. A., von Haeseler, A. & Minh, B. Q. IQ-TREE: a fast and effective stochastic algorithm for estimating maximum-likelihood phylogenies. *Mol. Biol. Evol*. **32**, 268–274 (2015).
62. Hoang, D. T., Chernomor, O., von Haeseler, A., Minh, B. Q. & Vinh, L. S. UFBoot2: improving the ultrafast bootstrap approximation. *Mol. Biol. Evol*. **35**, 518–522 (2018).
63. Mitchell, A. L. et al. InterPro in 2019: improving coverage, classification and access to protein sequence annotations. *Nucleic Acids Res*. **47**, D351–D360 (2019).
64. Waterhouse, A. et al. SWISS-MODEL: homology modelling of protein structures and complexes. *Nucleic Acids Res*. **46**, W296–W303 (2018).
65. Rose, A. S. & Hildebrand, P. W. NGL Viewer: a web application for molecular visualization. *Nucleic Acids Res*. **43**, W576–W579 (2015).
66. Benkert, P., Biasini, M. & Schwede, T. Toward the estimation of the absolute quality of individual protein structure models. *Bioinformatics* **27**, 343–350 (2011).
67. Korber, B. in *Computational Analysis of HIV Molecular Sequences* Ch. 4 (eds Rodrigo, A. G. & Learn, G. H.) 55–72 (Kluwer Academic Publishers, 2000).
68. Leskovec, J. SNAP 2.1. http://snap.stanford.edu/snap-2.1/download.html (2013).

Acknowledgements We thank D. Hyeroba, K. Swaibu and J. Carag for assistance in the field; C. Langner and the zoo in Germany for assistance with sampling and for implementing timely response strategies; L. Bollinger, J. Wada and D. Rubbenstroth for their help improving the manuscript and figures; G. K. Rice for advice and assistance with bioinformatics scripts; P. Zitzow J. Lorke, S. Schuparis and G. Czerwinski for technical assistance; and C. Jelinek, D. Kaufmann, J. Pöhlig and C. Trapp for help with rodent trapping and dissection. This work was supported in part through US National Institute of Allergy and Infectious Diseases (NIAID) Virology Training Grants T32 AI078985 (to University of Wisconsin-Madison) and GEIS P0062_20_NM_06 (to K.A.B.-L.), and by the Federal Ministry of Education and Research within the research consortium ‘ZooBoCoi’ (01KI1722A). This work was also partially supported through the prime contract of Laulima Government Solutions with NIAID under contract no. HHSN272201800013C and Battelle Memorial Institute’s former prime contract with NIAID under contract no. HHSN272200700016I. J.H.K. performed this work as a former employee of Battelle Memorial Institute and a current employee of Tunnell Government Services (TGS), a subcontractor of Laulima Government Solutions under contract no. HHSN272201800013C. Additional support was provided through the German Center for Infection Research (DZIF) TTU ‘Emerging Infections’ (to R.G.U.), and by the University of Wisconsin-Madison Global Health Institute, Institute for Regional and International Studies, and John D. MacArthur Professorship Chair (to T.L.G.). The views and conclusions contained in this document are those of the authors and should not be interpreted as necessarily representing the official policies or positions, either expressed or implied, of the US Department of Health and Human Services, Department of the Navy, Department of Defense, US Government, or any of the institutions and companies affiliated with the authors. In no event shall any of these entities have any responsibility or liability for any use, misuse, inability to use, or reliance upon the information contained herein. The US departments do not endorse any products or commercial services mentioned in this publication. K.A.B.-L. is an employee of the US Government. This work was prepared as part of her official duties. Title 17 U.S.C. § 105 provides that ‘Copyright protection under this title is not available for any work of the United States Government.’ Title 17 U.S.C. § 101 defines a U.S. Government work as a work prepared by a military service member or employee of the U.S. Government as part of that person’s official duties. The study protocol was reviewed and approved by the University of Wisconsin-Madison Institutional Animal Care and Use Committee in compliance with all applicable federal regulations governing the protection of animals and research.

Author contributions A.J.B., A.C.P., A.E., J.H.K., K.A.B.-L., M.B. and T.L.G. contributed to the study conception and design. A.B., A.J.B., A.C.P., A.E., E.H., G.P., K.A.B.-L., M.B., R.G.U. and T.L.G. contributed to sample and data collection. A.B., A.J.B., A.C.P., A.E., F.P., D.H., E.H., J.H.K., K.A.B.-L., M.B., R.G.U. and T.L.G. contributed to data analyses, interpretation and writing. All authors read and approved the final manuscript.

Competing interests The authors declare no competing interests.

Additional information

Supplementary information is available for this paper at https://doi.org/10.1038/s41586-020-2812-9.

Correspondence and requests for materials should be addressed to M.B. or T.L.G.

Peer review information *Nature* thanks Peter Daszak, Fabian Leendertz and the other, anonymous, reviewer(s) for their contribution to the peer review of this work.

Reprints and permissions information is available at http://www.nature.com/reprints.

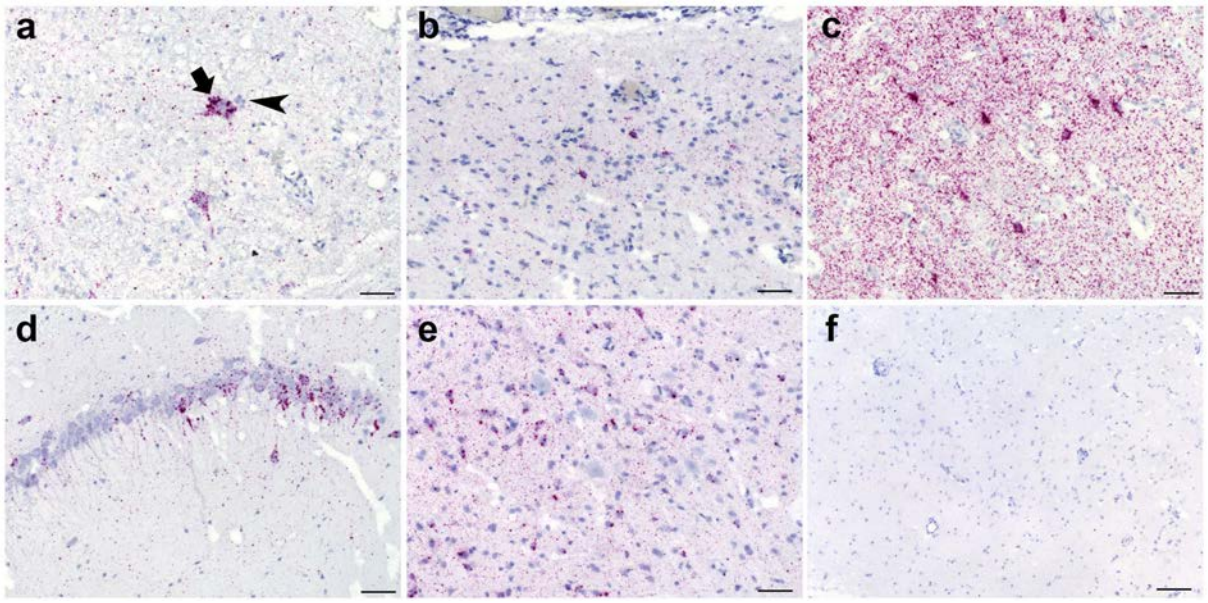

Extended Data Fig. 1 | RNA in situ hybridization of RusV. a–e, Detection of RusV RNA using in the brain tissues of a donkey (**a**), red-necked wallaby (**b**), capybara (**c**) and yellow-necked field mice (**d**, **e**). Chromogenic labelling (fast red) with probes against the NSP-coding region of RusV are visible in neuronal cell bodies (arrow) but not in adjacent glial cells (arrowhead). Scale bars, 50 µm. **f**, Negative control probe against the bacterial gene *dapB*, which encodes dihydrodipicolinate reductase. Lack of chromogenic labelling (fast red). Scale bar, 100 µm. All sections were counterstained with Mayer's haematoxylin.

RNAscope results were evaluated on at least three slides per animal, yielding comparable results in all cases. In situ hybridization was performed according to the manufacturer's instructions, including a positive control probe against peptidylprolyl isomerase B (cyclophilin B) and a negative control probe against dihydrodipicolinate reductase (DapB). Evaluation and interpretation were performed by a board-certified pathologist (DiplECVP) with more than 13 years of experience.

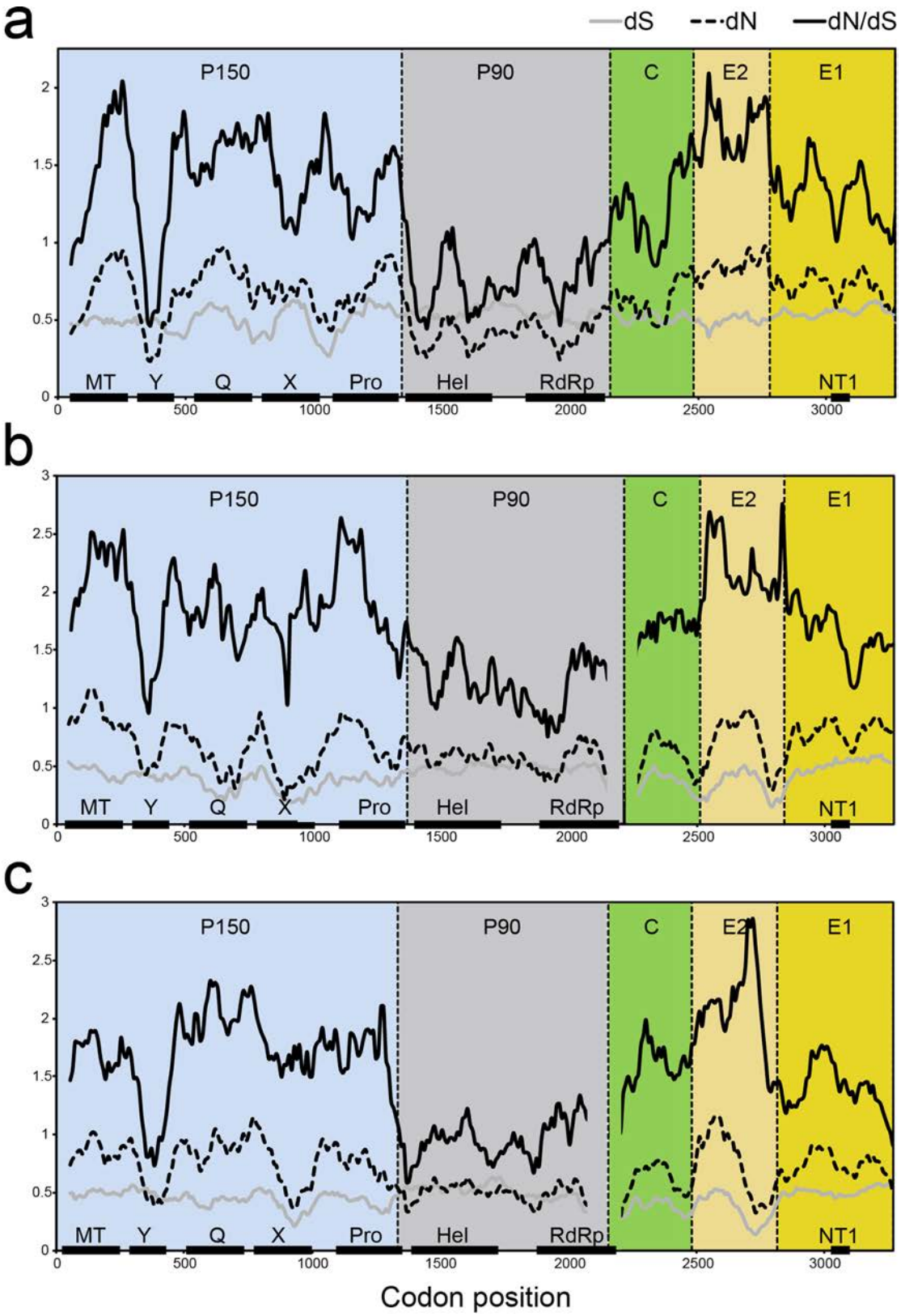

Extended Data Fig. 2 | Average substitution rates at non-synonymous and synonymous sites, and the ratio of dN/dS for aligned, concatenated amino acid sequences. a–c, The average substitution rates at non-synonymous (dN; dashed lines) and synonymous (dS; grey lines) sites, and the ratio of dN/dS (solid lines) for aligned, concatenated amino acid sequences were compared for RuV and RuhV (**a**), RuV and RusV (**b**), and RuhV and RusV (**c**) using sliding windows (100-residue window length, 10 residue steps). Protein domains are labelled on the *x* axes. MT, methyltransferase; Y, Q and X, domains of unknown function; Pro, protease; Hel, helicase; RdRp, RNA-directed RNA polymerase; NT1, neutralizing epitope 1.

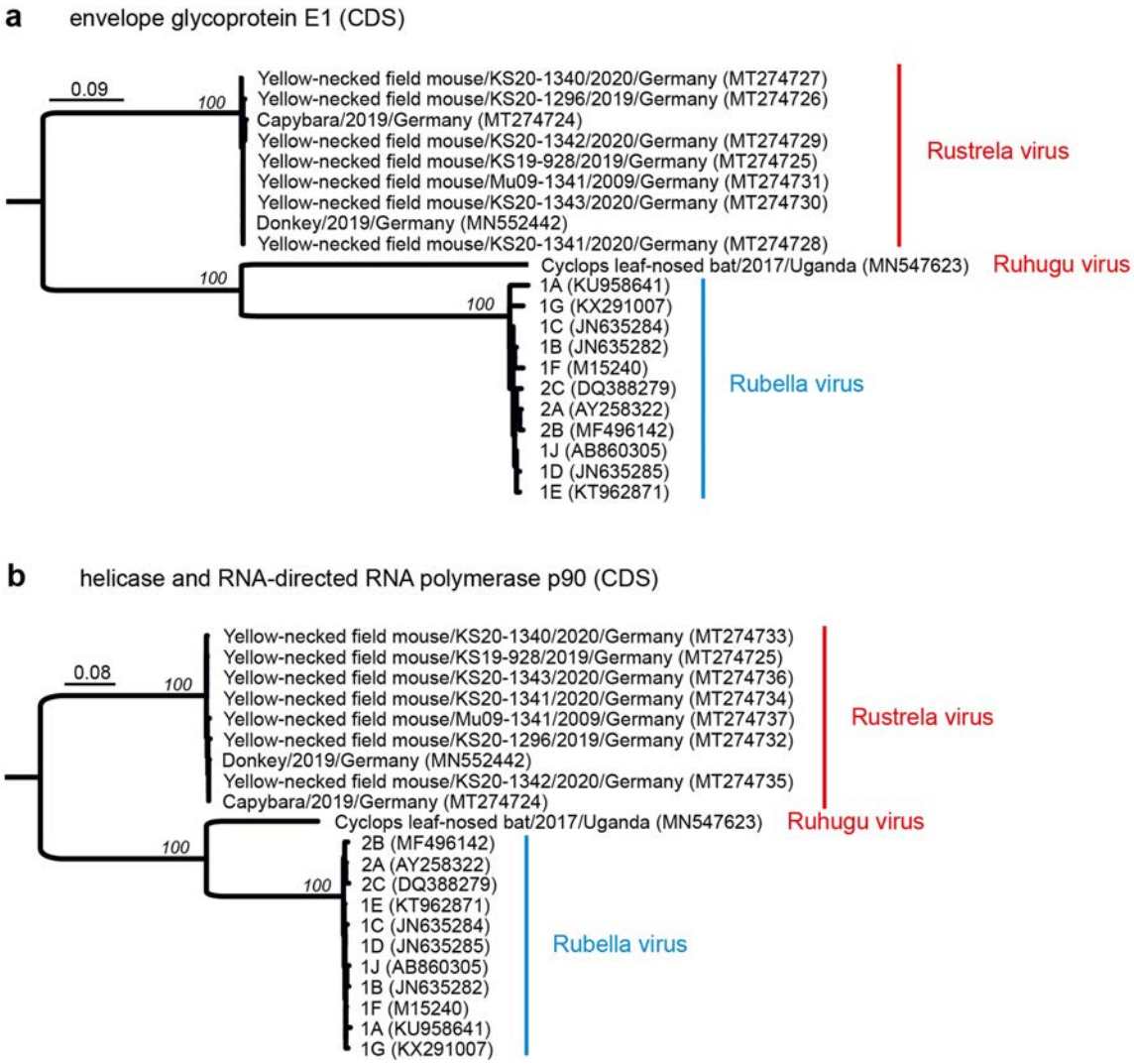

Extended Data Fig. 3 | Phylogenetic analyses of the coding sequences of envelope glycoprotein E1, and the helicase and RNA-directed RNA polymerase p90. a, **b**, Phylogenetic analyses of the coding sequences (CDS) of the envelope glycoprotein E1 (**a**) and the helicase and RNA-directed RNA polymerase p90 (**b**) of RuV, RuhV and RusV, including all sequences obtained in this study (GenBank accession numbers are listed in parentheses). Numbers above branches represent bootstrap values; scale bars indicate amino acid substitutions per site.

Extended Data Table 1 | RusV in small mammals from northeastern Germany

Common name	*Species*	*Capture location*		*Total*
		Zoo	*Within 10 km of zoo*	
Yellow-necked field mouse	*Apodemus flavicollis* [Melchior, 1834]	6/11 (54.5 %)	2/5 (40 %)	8/16 (50 %)
Striped field mouse	*Apodemus agrarius* [Pallas, 1771]	0/4	0/2	0/6
Bank vole	*Myodes glareolus* [Schreber, 1780]	0/3	-	0/3
Brown rat	*Rattus norvegicus* [Berkenhout, 1769]	0/13*	-	0/13
House mouse	*Mus musculus* Linnaeus, 1758	0/3*	0/13	0/16

Presence of the virus in the tissues was assessed by RTñqPCR. ≠, no material available.
*Two brown rats and all three house mice were housed at the zoo.

Extended Data Table 2 | RusV distribution in tissues from zoo animals

		Cq value		
	Source	*Donkey*	*Capybara*	*Red-necked wallaby*
Central nervous system	Cerebrum (I)[a]	22.9	-	30.2
	Cerebrum (II)[b]	29.2	26.0	-
	Cerebrum (III)[b]	29.5	26.6	-
	Cerebrum (IV)[b]	-	30.9	-
	Brain stem[b]	30.5	29.1	-
	Cerebellum[b]	30.6	-	-
	Medulla oblongata[b]	33.9	-	-
	Medulla[b]	-	34.6	-
	Spinal cord[b]	-	30.7	-
Peripheral organs	Liver (I)[a]	-	-	-
	Liver (II)[b]	35.9	-	-
	Kidney[b]	neg	neg	-
	Spleen[b]	neg	neg	-
	Small intestine[b]	-	neg	-
	Organ pool (I)[a]	neg	-	35.5
	Organ pool (II)[a]	-	-	-

Presence of the virus in the tissues was assessed by RTñqPCR. ≠, no material available; neg, negative. Cells are shaded in proportion to the relative viral concentration (C_q value).

[a]Fresh, unfixed tissues.

[b]FFPE tissues.

Extended Data Table 3 | RusV distribution in tissues of *A. flavicollis*

	Cq value								
	KS19/923	*KS20/926*	*KS19/928*	*KS20/1296*	*KS20/1340*	*KS20/1341*	*KS20/1342*	*KS20/1343*	*Mu09/1341*
Cerebrum	28.1	neg	22.9	24.1	26.3	21.1	20.8	20.4	25.9
Heart	neg	neg	neg	neg	31.9	neg	neg	neg	-
Lungs	neg	neg	neg	neg	36.7	35.0	neg	neg	-
Liver	neg	neg	neg	neg	neg	neg	neg	neg	-
Kidneys	neg	neg	neg	neg	neg	neg	neg	neg	-
Spleen	neg	neg	neg	neg	neg	neg	neg	neg	-
Intestine/feces	neg	36.7	neg	neg	neg	neg	neg	neg	-
Thoracic lavage	neg	neg	neg	neg	37.5	neg	neg	neg	-
Oral swab	-	-	-	-	36.2	37.5	neg	neg	-

Presence of the virus in the tissues was assessed by RTñqPCR. ≠, no material available; neg, negative. Cells are shaded in proportion to the relative viral concentration (C_q value).

Extended Data Table 4 | Genomic features of RuhV and RusV

Genome feature[c]	*Nucleotide position (5'→3')*		*Amino acid residues*		*Amino acid sequence identity (%)*			*GC content (%)*		
	RuhV	*RusV*	*RuhV*	*RusV*	*RuhV*[a]	*RusV*[a]	*RuhV–RusV*	*RuhV*	*RusV*	*RuV*[b]
Complete genome	1–9621	1–9322	6296	5876	56.4	43.0	43.3	63.5	70.6	69.6
Non-structural polyprotein	44–6190	68–5833	2049	1921	59.0	45.9	47.5	62.2	70.2	70.0
p150 protease	44–3754	68–3391	1237	1108	48.6	34.5	35.7	63.1	72.0	71.4
p90 replication complex	3755–6190	3392–5830	812	813	75.7	65.5	66.6	60.9	67.7	67.8
Structural polyprotein	6266–9562	6193–9246	1099	1017	51.4	41.1	39.5	66.1	71.4	69.4
Capsid protein	6266–7216	6193–6807	317	205	51.7	46.6	43.0	66.6	74.5	73.1
E2 envelope protein	7217–8101	6808–7785	295	326	43.6	31.4	23.9	67.9	72.7	71.0
E1 envelope protein	8102–9562	7786–9243	487	486	56.3	51.0	50.6	64.8	69.3	66.3

[a]Inferred amino acid sequence identities of RuhV (GenBank MN547623) and RusV (GenBank MN552442) compared to RuV strain F≠Therien (RefSeq NC_001545).
[b]GC content is shown for RuV strain F≠Therien (RefSeq NC_001545).

Extended Data Table 5 | Conservation of B and T cell epitopes in E1 fusion proteins

	Epitope	Rubella virus (JN635282)	Ruhugu virus (MN547623)	Rustrela virus (MN552442)
Linear, neutralizing B-cell epitopes	NT1:$E1_{1221-239}$	LGSPNCHGPDWASPVCQRHS	**V**G**L**PNCHGPDWASPVCQ**Q**HS	**V**<u>**P**</u>**A**P**D**C**F**GP**A**WASPVC**A**RH**M**
	NT2: $E1_{245-251}$	LVGATPE	L**T**G**VP**PE	L**T**GATP**G**
	NT3 :$E1_{260-266}$	ADDPLLR	ADDP**RL**T	ADD**LGWH**
	NT4 :$E1_{274-285}$	VWVTPVIGSQAR	VW**A**V**A**V**K**GT**Q**P**K**	VW**YQ**PVIG**R**Q**P**R
CD8⁺ T-cell epitopes	C_{9-22}	MEDLQKALEAQSRA	**LA**DLQ**RL**LE**K**QS**AE**	Deleted
	C_{11-29}	DLQKALEAQSRALRAELAA	DLQ**RL**LE**K**QS**AE**LRAE**M**A**R**	Deleted
	$C_{264-272}$	RIETRSARH	**KQDVKSDKV**	R**K**E<u>QLG</u>**ATSGAA**

The E1 fusion proteins of the wild-type RuV 1B, RuhV and RusV are compared. Differences in the amino acid sequence are highlighted in bold and insertions are underlined. GenBank accession numbers are indicated in parentheses.

Extended Data Table 6 | Immunohistochemical markers and applications

Marker	*Antibody*	*Antigen Retrieval*	*Secondary reagents*
Active caspase 3	Anti-Active Caspase 3 (Promega, Walldorf, Germany), 1:200, overnight	n/a	ABC Kit Vectastain Elite PK 6100, 30 min (Dako)
CD79a	Mouse anti-CD79A (clone HM57) monoclonal, (LifeSpan BioSciences, Seattle, WA, USA), 1:50, overnight	HIER, 10 mM Tris/1mM EDTA buffer pH 9.0, 20 min	Dako EnVision+ System-HRP Labelled Polymer Anti-mouse, 30 min
CD3	Rabbit anti-CD3 polyclonal (Dako), 1:100, overnight	HIER, 10 mM Tris/1mM EDTA buffer pH 9.0, 20 min	Dako EnVision+ System- HRP Labelled Polymer Anti-rabbit, 30 min
Iba-1	Iba1 (Wako), 1:800, overnight	HIER, Citrate buffer pH 6.0, for 20 min	Dako EnVision+ System- HRP Labelled Polymer Anti-rabbit, 30 min

HIER, heat-induced epitope retrieval; HRP, horseradish peroxidase; n/a, not applicable.

nature research

Corresponding author(s): Tony L. Goldberg

Last updated by author(s): 10th June, 2020

Reporting Summary

Nature Research wishes to improve the reproducibility of the work that we publish. This form provides structure for consistency and transparency in reporting. For further information on Nature Research policies, see Authors & Referees and the Editorial Policy Checklist.

Statistics

For all statistical analyses, confirm that the following items are present in the figure legend, table legend, main text, or Methods section.

n/a	Confirmed
☐	☒ The exact sample size (*n*) for each experimental group/condition, given as a discrete number and unit of measurement
☒	☐ A statement on whether measurements were taken from distinct samples or whether the same sample was measured repeatedly
☐	☒ The statistical test(s) used AND whether they are one- or two-sided *Only common tests should be described solely by name; describe more complex techniques in the Methods section.*
☒	☐ A description of all covariates tested
☒	☐ A description of any assumptions or corrections, such as tests of normality and adjustment for multiple comparisons
☐	☒ A full description of the statistical parameters including central tendency (e.g. means) or other basic estimates (e.g. regression coefficient) AND variation (e.g. standard deviation) or associated estimates of uncertainty (e.g. confidence intervals)
☒	☐ For null hypothesis testing, the test statistic (e.g. *F*, *t*, *r*) with confidence intervals, effect sizes, degrees of freedom and *P* value noted *Give P values as exact values whenever suitable.*
☒	☐ For Bayesian analysis, information on the choice of priors and Markov chain Monte Carlo settings
☒	☐ For hierarchical and complex designs, identification of the appropriate level for tests and full reporting of outcomes
☒	☐ Estimates of effect sizes (e.g. Cohen's *d*, Pearson's *r*), indicating how they were calculated

Our web collection on statistics for biologists contains articles on many of the points above.

Software and code

Policy information about availability of computer code

Data collection	For RuhV, sequencing was performed using Illumina NextSeq 500 v2 chemistry and Illumina MiSeq v3 chemistry. Non-viral and low quality reads were removed using FastQC v0.11.5, bbmap v37.78, and bbduk v37.78. For RusV, sequencing was performed using Thermo Fischer Ion S5 XL System with a 530 chip and Illumina MiSeq v3 chemistry. Host reads were removed using BWA (no version number is applicable to BWA), and low quality reads were removed using 454 software suite version 3.0 and FastQC v0.11.5. E2 protein hydrophobic domains were detected using ProtScale (no version number is applicable to ProtScale). Primer and probe specificity for RusV RT-qPCR were verified by BLASTN.
Data analysis	For RuhV, De novo assembly of sequence reads was performed using MetaSPAdes version 3.7 and CLC Genomics Workbench version 12.0. Viral contigs were identified using the VirusSeeker discovery pipeline (no version is applicable to VirusSeeker). Contigs were assigned to taxa by DIAMOND (no version is applicable for DIAMOND) using the BLASTX algorithm. For RusV, mapping and assembly of reads were performed using the 454 software suite version 3.0, SPAdes v3.12.0, Bowtie 2 v2.3.5, and Geneious version 11.1.5. Reads were initially assigned to taxa using the RIEMS software pipeline (no version is applicable to RIEMS), and RuhV-specific contigs were identified by DIAMOND (no version is applicable to DIAMOND). Phylogenetic trees were inferred using IQ-TREE version 1.6.12. Protein functional domain prediction and annotation were performed using the InterPro webserver (no version), and the confidence of structural homology comparisons were estimated using Phyre2.

For manuscripts utilizing custom algorithms or software that are central to the research but not yet described in published literature, software must be made available to editors/reviewers. We strongly encourage code deposition in a community repository (e.g. GitHub). See the Nature Research guidelines for submitting code & software for further information.

Data

Policy information about availability of data

All manuscripts must include a data availability statement. This statement should provide the following information, where applicable:

- Accession codes, unique identifiers, or web links for publicly available datasets
- A list of figures that have associated raw data
- A description of any restrictions on data availability

Sequence data that support the findings of this study have been deposited in GenBank with the accession numbers MN547623, MN552442, and MT274724-MT274737

Field-specific reporting

Please select the one below that is the best fit for your research. If you are not sure, read the appropriate sections before making your selection.

☒ Life sciences ☐ Behavioural & social sciences ☐ Ecological, evolutionary & environmental sciences

For a reference copy of the document with all sections, see nature.com/documents/nr-reporting-summary-flat.pdf

Life sciences study design

All studies must disclose on these points even when the disclosure is negative.

Sample size	Sample sizes of bats and rodents were based on statistical power analysis. Specifically, 19 individuals of each type was calculated to yield a 95% probability of detecting at least one infected individual assuming a prevalence of 15%, based on the binomial distribution. The fact that 50% of individuals were, in fact, positive in each case illustrates that our sample sizes were actually well in excess of what was needed.
Data exclusions	No data were excluded from the analyses.
Replication	Samples were sequenced twice and results were compared directly for confirmation. No discrepancies between replicates were noted. Immunohistochemistry was performed on at least 10 slides per animal yielding comparable results. In each run, the tissues were tested in parallel for unspecific labeling using a primary control antibody. Additionally, for each antibody and staining (Prussion blue) applied, we included a positive control slide in each run. H&E and immunohistochemistry evaluation and interpretation was performed by a board certified pathologist (DiplECVP) with more than 13 years experience. In situ hybridization was performed according to the manufacturer's instructions including a positive control probe peptidylprolyl isomerase B (cyclophilin B, ppib) and a negative control probe dihydrodipicolinate reductase (DapB). Results were universally consistent among slides and conformed to expectations of the positive and negative control probes.
Randomization	Randomization was not relevant to this study because this was not an experimental study, but rather a study of the natural occurrence of a group of viruses.
Blinding	Blinding was not relevant to this study because this was not an experimental study, but rather a study of the natural occurrence of a group of viruses.

Reporting for specific materials, systems and methods

We require information from authors about some types of materials, experimental systems and methods used in many studies. Here, indicate whether each material, system or method listed is relevant to your study. If you are not sure if a list item applies to your research, read the appropriate section before selecting a response.

Materials & experimental systems

n/a	Involved in the study
☒	☐ Antibodies
☒	☐ Eukaryotic cell lines
☒	☐ Palaeontology
☐	☒ Animals and other organisms
☒	☐ Human research participants
☒	☐ Clinical data

Methods

n/a	Involved in the study
☒	☐ ChIP-seq
☒	☐ Flow cytometry
☒	☐ MRI-based neuroimaging

Animals and other organisms

Policy information about studies involving animals; ARRIVE guidelines recommended for reporting animal research

Laboratory animals	The study did not involve laboratory animals.

Wild animals	20 cyclops leaf-nosed bats (9 males and 11 females) in Uganda were caught in mist nets set in their flight path as they exited tree roosts at dusk and were kept in cloth bags until processing. Oral swabs were collected from each bat using sterile swabs and preserved in 500 µl of TRI Reagent. Bats were held in cloth bags until processing and released immediately thereafter at the site of capture. In Germany, tissues were acquired from a local zoo where a red-necked wallaby, a donkey, and a capybara had died of encephalitis. Tissues from these animals were provided to the Friedrich Loeffler Institute for diagnostic evaluation. In addition, tissues from 54 wild rodents (28 males and 26 females) were obtained as a result of rodent control efforts instituted at a zoo and from tissue archives available from other ongoing research. These animals were killed either directly by trapping (rodent control measures) or using cotton balls with isofluorane (ongoing field studies).
Field-collected samples	Bat oral swabs collected in Uganda were frozen at -20 °C within 3 h of sample collection and transported on ice for storage at -80 °C for ~6 months prior to further analyses. Tissues from the red-necked wallaby, donkey and capybara were provided immediately to the diagnostic laboratory of the Friedrich Loeffler Institute, where they were either frozen fresh at -80 °C for ~9 months prior to analysis or prepared immediately for histopathology by formalin fixation and imbedding in paraffin. For small mammals in Germany, tissues were stored on ice in the field, and sections were frozen within 6 hours of collection at -80 degrees and prepared for histopathology by formalin fixation and imbedding in paraffin and stored for an average of 7 months prior to analysis.
Ethics oversight	Animal collection and handling protocols were approved by the Uganda Wildlife Authority, the Uganda National Council for Science and Technology, and the University of Wisconsin-Madison Animal Care and Use Committee. Samples were shipped in accordance with international law and imported under PHS permit number 2017-07-103 issued by the US Centers for Disease Control and Prevention, Atlanta, GA, USA. Protocols in Germany were approved by the institutional animal care and use committee of the Friedrich Loeffler Institute.

Note that full information on the approval of the study protocol must also be provided in the manuscript.